Nanoscale

PAPER

View Article Online
View Journal | View Issue

Cite this: *Nanoscale*, 2023, **15**, 9040

A combined theoretical and experimental investigation on the photocatalytic hydrogenation of CO_2 on Cu/ZnO polar surface†

Han Xiao, [a,b] Yihong Lian,[a] Shiduo Zhang, [a] Minyi Zhang, *[a,b] Jiye Zhang *[c] and Chunsen Li *[a,b,d,e]

The photocatalytic hydrogenation of CO_2 by Cu-deposited ZnO (Cu/ZnO) polar surfaces is investigated through density functional theory (DFT) calculations combined with experimental work. The DFT results demonstrate that, without Cu-loading, CO_2 and H_2 present weak physisorption on the clean ZnO polar surface, except that H_2 undergoes strong chemisorption on the ZnO(000$\bar{1}$) surface. Cu deposition on the ZnO polar surface could remarkably enhance the CO_2 chemisorption ability, due to the induced charge redistribution on the interface of the Cu/ZnO polar surface systems. Additionally, a Cu-nanoisland, which was simulated using a Cu(111) slab model, exhibited strong ability to chemically adsorb H_2. Thus, H_2 may act as an adsorption competitor to CO_2 on the Cu/ZnO(000$\bar{1}$), while, in contrast, CO_2 and H_2 (syngas) may have more opportunity to simultaneously adsorb on Cu/ZnO(0001) to promote the CO_2 hydrogenation. These facet-dependent properties lead us to assume that Cu/ZnO(0001) should be a favorable photocatalyst for CO_2 hydrogenation. This assumption is further verified by our photocatalysis experiment based on a ZnO single crystal. According to the theoretical and experimental results, the optimal HCOO* reaction pathway for the photocatalytic hydrogenation of CO_2 on Cu/ZnO(0001) is proposed. In this optimal HCOO* path, the hydrogenation of CO_2* step and hydrogenation of HCOO* step could be promoted by the coupling of a photo-generated spillover proton and a photoelectron on the interface of Cu/ZnO(0001). This research demonstrates the feasibility of the photocatalytic reduction of CO_2 on Cu/ZnO(0001), and will help to develop related high-efficiency catalysts.

Received 3rd March 2023,
Accepted 21st April 2023

DOI: 10.1039/d3nr01001e

rsc.li/nanoscale

1. Introduction

From the perspective of reducing the concentration of carbon dioxide in the atmosphere to combat the greenhouse effect and global warming, the conversion of carbon dioxide into chemical feedstocks such as formic acid and methanol through catalytic hydrogenation is an important strategy.[1–4] Solid catalysts such as the transition-metal-doped zinc oxide (ZnO) exhibit high activity and selectivity for the reduction of CO_2, and have been considered as key chemical platforms for the production of fuels and feedstocks at pressures less than 100 bar and temperatures ranging from 473 to 573 K.[5–7] However, compared with conventional catalytic strategies, photocatalytic CO_2 hydrogenation is now becoming a new promising green chemistry technology that can directly convert CO_2 into useful chemical products under ultraviolet and visible light irradiation without high temperature and high pressure conditions.[8–10] ZnO has been extensively investigated as a photocatalyst for solar energy conversion and organic or dye pollutant treatment due to its excellent electrochemical stability, high electron mobility, and photocatalytic efficiency.[11–14] The polar surfaces of ZnO, such as the Zn-terminated surface ZnO(0001) and O-terminated surface ZnO (000$\bar{1}$), were found to be more active in photocatalytic reactions than the nonpolar surfaces of ZnO,[15–17] because the dipoles associated with Zn- and O-terminated surfaces cause electrostatic instability on these surfaces. As such, much research work has been devoted to development of efficient photocatalysts for CO_2 reduction using ZnO as an important composite.[18–21]

[a]*State Key Laboratory of Structural Chemistry, Fujian Institute of Research on the Structure of Matter, Chinese Academy of Sciences, Fuzhou, Fujian 350002, China. E-mail: myzhang@fjirsm.ac.cn, Chunsen.li@fjirsm.ac.cn*
[b]*University of Chinese Academy of Sciences, Beijing 100049, China*
[c]*School of Materials Science and Engineering, Shanghai University, Shanghai 200444, China. E-mail: jychang@shu.edu.cn*
[d]*Fujian Provincial Key Laboratory of Theoretical and Computational Chemistry, Xiamen University, Xiamen, Fujian 361005, China*
[e]*Fujian College, University of Chinese Academy of Sciences, Fuzhou, Fujian 350002, China*

†Electronic supplementary information (ESI) available. See DOI: https://doi.org/10.1039/d3nr01001e

On the other hand, many studies have also focused on Cu-decorated ZnO, which generally exhibits reduced optical band-gap energy, increased optical absorption ability, and improved photocatalytic properties compared with bare ZnO.[22–25] Pawar *et al.* recently reported that Cu-doped ZnO microstructures showed enhanced performance in the photocatalytic degradation of methylene blue and rhodamine B dyes due to the existence of a large amount of (001) polar surfaces.[26] Moreover, Tsang *et al.* found that the exposed polar face (002) of Cu-deposited ZnO (Cu/ZnO) showed higher selectivity towards the hydrogenation of CO_2 to methanol compared with other crystal facets,[27] and thus demonstrated the important role of facet type in regulating catalytic reactivity.[28] This evokes speculation that the ZnO polar surface in synergy with copper might also exhibit good photocatalytic CO_2 hydrogenation ability.

It has been found that the interaction of the deposited Cu and ZnO has a significant impact on the activation and hydrogenation of CO_2.[5,6,29] However, little is known about the structure–activity relationship between deposited Cu and the polar surfaces of ZnO, such as the active sites, and the mechanism of CO_2 activation on polar surfaces. Moreover, no consensus has been reached on the adsorption behavior of CO_2 on ZnO (0001) and ZnO(000$\bar{1}$) polar surfaces in previous experimental and theoretical work.[26,27,30] Therefore, a detailed study of how CO_2 interacts with clean ZnO polar surfaces as well as Cu/ZnO polar surfaces will help to provide an understanding of the intrinsic mechanism of the photocatalytic hydrogenation of CO_2 by Cu/ZnO photocatalyst.

In the present paper, our study focuses on exploring the mechanism of the photocatalytic hydrogenation of CO_2 on the Cu-deposited ZnO polar surfaces, ZnO(0001) and ZnO(000$\bar{1}$). By performing theoretical simulations, we investigated the adsorption behaviors of CO_2 and H_2 on the polar surface of clean and Cu-deposited ZnO polar surfaces, respectively. The potential active polar surface, Cu/ZnO(0001), is proposed based on the elucidation of adsorption sites, relaxation geometries, and electrical properties, as we shall show. Then, DFT calculations were performed to investigate the reaction mechanism of CO_2 hydrogenation on the Cu/ZnO(0001) surface and the favorable reaction pathway in terms of energy was identified. Furthermore, illustrative experiments were done accordingly, and the results were in good agreement with the theoretical predictions. Finally, based on the combined theoretical and experimental works, we propose a possible reaction route for the direct photocatalytic hydrogenation of CO_2 on the Cu/ZnO surface.

2. Theoretical and experimental methods

2.1. Computational methods and modeling

All calculations were performed using the first-principles method based on density functional theory (DFT) and the first-principles pseudo-potential method to simulate the surface reconstruction and formation energy. The DFT calculations were carried out using the Vienna Ab Initio Simulation Package (VASP) code[31,32] with the projector-augmented wave (PAW) method using the Perdew–Burke–Ernzerhof (PBE) exchange–correlation functional[33,34] The GGA+U approximation with an effective Hubbard U-parameter U_{eff} = 7.65 eV was applied to describe the on-site Coulomb interaction among the localized zinc 3d electrons.[35] The value of U_{eff} is close to 7.5 eV, which was used in a similar Cu/ZnO system.[36] The plane wave cutoff was set as 400 eV, and the total energy convergence was set at 10^{-6} eV for self-consistent iterations. As shown in Fig. 1, the theoretical model used here consists of an orthogonal surface unit cell $a \times b$ (*i.e.*, 6.506 × 5.643 Å) containing four zinc and four oxygen atoms within each Zn–O layer in a repeated slab configuration. Each slab contains 6 Zn–O layers separated by a vacuum space of 20 Å. The surface sizes are $(1a \times 2b)$ corresponding to k-point meshes of $(4 \times 2 \times 1)$. In order to suppress any long-range interference between the zinc and oxygen-terminated ends of the slab, the dangling bonds of the bottom atoms of ZnO (0001) and (000$\bar{1}$) were saturated by adding one monolayer of pseudo-hydrogen atoms with a nuclear charge of $Z = 1/2|e|$ and $Z = 3/2|e|$, respectively. Only the top three Zn–O layers were relaxed, while the bottom three Zn–O layers were kept in their previously optimized crystal positions.

For the adsorption of Cu atoms and adsorbate molecules (CO_2 or H_2) on a clean ZnO polar surface, we simulated four symmetry adsorption sites, namely a top-site, bridge-site, fcc-site, and hcp-site (Fig. 1(b)). For the adsorption of CO_2 or H_2 on the Cu/ZnO system, four symmetry adsorption sites are also considered. The 1st–3rd positions are the edge site, the site close to the Cu atom, and the site far from the Cu atom, respectively (see Fig. 1(c)). The 4th adsorption site is a metallic site located far from the ZnO support. For simplified calculation, an ideal Cu(111) surface with a six-layer slab and a $p(4 \times 4)$ unit cell was used. In this model, only the top three layers

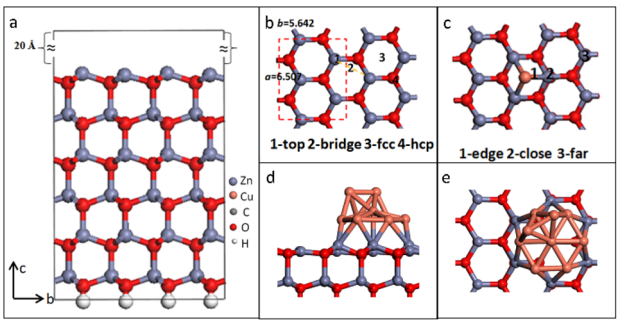

Fig. 1 (a) Side view of the slab supercell for the clean ZnO(0001) surface. (b) Top view of the slab supercell for the ZnO(0001) surface and the related CO_2/H_2 adsorption sites; top view of the slab supercell for the ZnO (0001) surface. (c) Top view of the slab supercell for the Cu/ZnO(0001) surface and the related CO_2/H_2 adsorption sites. (d) Side view and (e) top view of the slab supercell for the Cu_9/ZnO(0001) surface. Note: The geometry of ZnO (000$\bar{1}$) surface can be simply imaged by O atom and Zn atom interchange.

were relaxed, and k-point meshes of 4 × 4 × 1 were used. The energy of adsorption/binding E_{ad} is defined as:

$$E_{ad} = E_{ads/sub} - E_{ads} - E_{sub}$$

where $E_{ads/sub}$ is the total energy of the substrate covered with the adsorbate in the optimized configuration, and E_{ads} and E_{sub} are the total energies of the adsorbate in the gas phase and the relaxed clean substrate, respectively.

Moreover, we constructed the Cu_9 cluster loading on the ZnO(0001) surface with a size of $(4a \times 4b)$ and $(2 \times 2 \times 1)$ k point meshes to explore the CO_2 hydrogenation pathways (Fig. 1(d) and (e)). In this model, only the top two Zn–O layers were relaxed, while the bottom four Zn–O layers were kept on their previously optimized crystal positions. The starting geometry of the Cu_9/ZnO(0001) surface was first determined by running *ab initio* molecular dynamics (AIMD) using a Nose thermostat at a temperature of 300 K for 12 ps. The subsequent energy minimized snapshots extracted from the AIMD trajectories were then singled out and optimized.

2.2. Synthesis of Cu/ZnO polar surface photocatalysts and related characterization

Two pieces of (0001) facet oriented ZnO wafers with a size of 10 × 10 × 0.5 mm were cut from a bulk ZnO single crystal grown *via* a hydrothermal method[37] and then polished and cleaned. The determination of polarized facets was conducted using a simple chemical etching method.[38] Cu nanoislands were deposited on the ZnO wafers using a radiofrequency magnetron sputtering system. The diameter and thickness of the Cu target were 50 mm and 3 mm, respectively, and the purity was greater than 99.99%. The working pressure (Ar 99.99%) was 0.1 Pa and the substrate was maintained at 473 K during the film deposition. The distance from the target to the substrate was 9.0 cm. The sputtering time was about 20 s. One of the wafers was deposited with Cu nanoislands on its (001) facet using the magnetron sputtering method, thus forming the Cu–ZnO(0001) catalyst. The other wafer was deposited with Cu nanoislands on its $(000\bar{1})$ facet under the same deposition conditions, thus forming the Cu–ZnO$(000\bar{1})$ catalyst. The morphologies and distribution of Cu metal on the ZnO substrates were characterized using atomic force microscopy (AFM; Veeco Multimode, Nano scope Multimode IIIa). X-ray photoelectron spectroscopy (XPS) analysis was conducted on an ESCA-LAB 250 photoelectron spectrometer (Thermo Scientific) using an Al Kαradiation (1486.6 eV). Height images of the films were recorded using tapping-mode AFM. The photocatalytic hydrogenation of CO_2 experiment was carried out in a flowing atmosphere and at room temperature using a custom-built reactor (see details in the ESI†). A CO_2/H_2 reaction mixture with a molar ratio of 1 : 3 was fed at a rate of 300 stp mL min^{-1} (stp = standard temperature and pressure, T = 298 K, P = 101.3 kPa) through the catalyst bed. Before each test, the catalysts were pre-reduced *in situ* at 573 K for 2 h under the H_2 flow (20 stp mL min^{-1}). The catalysts were illuminated using a 300 W Xe light source (Solaredge700, Beijing Perfect light Co. Ltd) for 4 h. The possible residual products on the surface of the catalysts were determined using a PerkinElmer system 2000 FT-IR spectrometer. A resolution of 4.0 cm^{-1} was used throughout the investigation and 50 scans taken over a 20 s interval were averaged to achieve a satisfactory signal-to-noise ratio.

3. Results and discussion

3.1. Geometries of Cu/ZnO polar surfaces and their adsorption properties toward CO_2/H_2

The models of the clean ZnO(0001)/$(000\bar{1})$ surface were simulated using slab models based on optimized bulk wurtzite ZnO using an orthogonal unit cell.[39] The performances of ZnO polar surfaces with copper deposition were simplistically simulated using one Cu atom deposited on the clean ZnO(0001) and ZnO$(000\bar{1})$ polar surfaces, respectively (see Fig. 2(a) and (b)). The calculated binding energies of the four high-symmetry deposition sites (*i.e.*, top, bridge, fcc-hollow, and hcp-hollow, as shown in Fig. 1(b)) are displayed in Table S1 (see ESI†). Our results found that both the ZnO(0001) surface and ZnO$(000\bar{1})$ surface could strongly bind to the Cu atom. For both the ZnO(0001) surface or ZnO$(000\bar{1})$ surface, the fcc-hollow site was the most stable deposition site for Cu.

Further, we investigated CO_2 and H_2 adsorption on the clean and Cu-deposited ZnO polar surfaces (see Fig. S1 and S2 in ESI†). Based on our calculations, only weak physisorption of CO_2 was found on the two clean polar surfaces (see Table S1† and the stable adsorption states of CO_2 on the two clean surfaces, Fig. 2(c) and (e)), which is in line with previous theoretical studies.[40] In contrast, H_2 adsorption on the ZnO polar surfaces showed facet-dependent properties. For the sites of ZnO(0001), H_2 adsorption only resulted from the physisorption of H_2. However, for the ZnO$(000\bar{1})$ surface, H_2 adsorption on the bridge-site and fcc-site could lead to strong chemisorption of H_2. In these cases, the H–H bond of H_2 is broken, and two dissociated H atoms are separately bound to two adjacent surface O atoms of the ZnO$(000\bar{1})$ surface.

The characteristics of CO_2 and H_2 adsorption on the Cu/ZnO polar surfaces were investigated by using the most stable Cu/ZnO polar surface with Cu deposited on the fcc-hollow site of the ZnO polar surface (see Fig. S2 in ESI†). The calculated adsorption energies with different deposition sites are listed in Table 1. In addition, in order to simulate the top of the deposited Cu nano-islands on the ZnO polar surfaces in the experiments, both the metallic sites of Cu/ZnO(0001) and Cu/ZnO$(000\bar{1})$ were simplified and simulated using the Cu(111) slab models (see Fig. 2(k) and (l)).

For the Cu/ZnO(0001) surface, CO_2 adsorption on the edge site has the lowest adsorption energy of −0.89 eV (see Table 1 and Fig. 2(g)). In this case, the linear CO_2 is bent to a bidentate carbonate with an internal angle O–C–O of 126.8°. Its C atom bonds to the Cu atom with C–Cu bond length of 1.98 Å, and one of its O atoms bonds to a surface Zn atom with an O–Zn bond length of 1.96 Å (see Fig. 2(g)). In the case of the Cu/ZnO$(000\bar{1})$ surface, CO_2 adsorption on the edge-site of Cu/ZnO

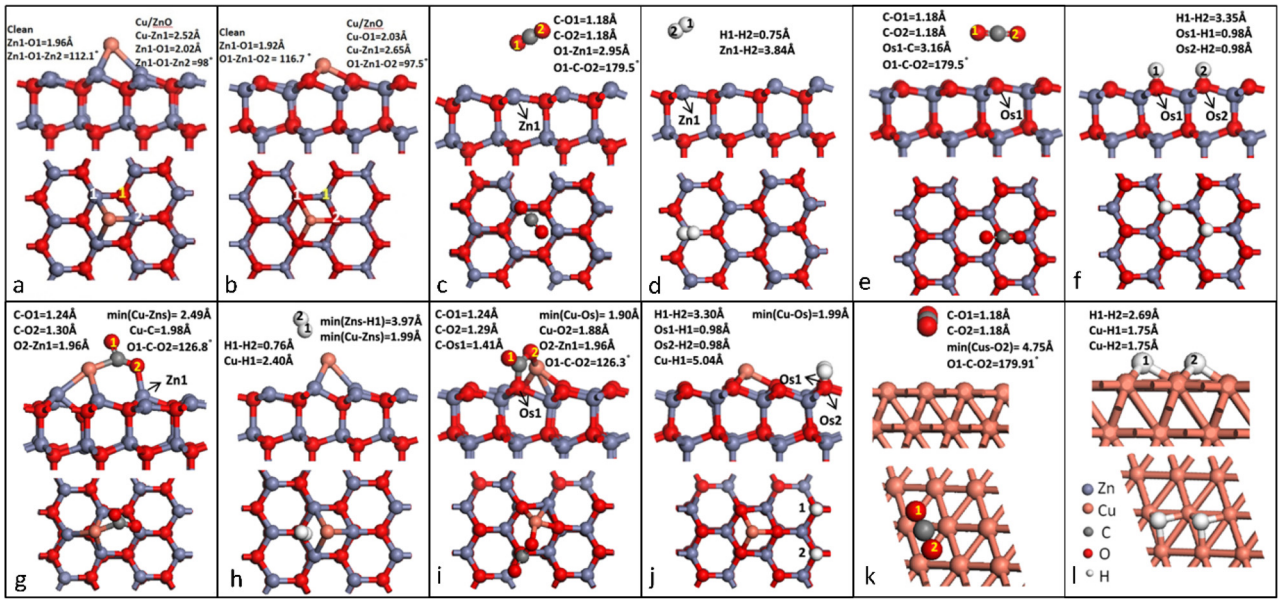

Fig. 2 The most stable geometry of Cu deposited at the fcc-site for (a) the clean ZnO(0001) and (b) ZnO(000$\bar{1}$) surfaces. The most stable geometry of (c) CO_2 and (d) H_2 adsorbed on the clean surface of ZnO(0001); and the most stable geometry of (e) CO_2 and (f) H_2 adsorbed on the clean surface of ZnO(000$\bar{1}$). The most stable geometry of (g) CO_2 and (h) H_2 adsorbed on Cu/ZnO(0001); the most stable geometry of (i) CO_2 and (j) H_2 adsorbed on the Cu/ZnO(000$\bar{1}$) system; the most stable geometry of (k) CO_2 and (l) H_2 adsorbed on metallic Cu(111).

Table 1 Adsorption energies (in eV) for CO_2 and H_2 adsorbed on the Cu/ZnO(0001) and Cu/ZnO(000$\bar{1}$) system

Cu/ZnO system	Edge	Close	Far	Metallic
(0001)/CO_2	−0.89	−0.06	−0.05	−0.03
(0001)/H_2	−0.05	−0.02	−0.02	−0.41
(000$\bar{1}$)/CO_2	−0.66	−0.58	−0.08	−0.03
(000$\bar{1}$)/H_2	−3.57	−4.45	−4.67	−0.41

(000$\bar{1}$) also leads to the lowest adsorption energy of −0.66 eV (see Table 1 and Fig. 2(i)). In this structure, the C atom of CO_2 binds with the O-terminated facet with a C–O bond length of 1.41 Å, and one of its O atoms bonds to the Cu atom with the Cu–O bond length of 1.88 Å. The internal O–C–O angle of CO_2 is bent to 126.3°. Thus, Cu deposition on ZnO polar surfaces would highly activate the CO_2 and promote the chemisorption of CO_2. Moreover, the chemisorption of CO_2 occurs only in close proximity to the Cu deposition sites of Cu/ZnO(0001) and Cu/ZnO(000$\bar{1}$) surfaces. For the far-sites and metallic sites of Cu/ZnO(0001) and Cu/ZnO(000$\bar{1}$), the adsorption of CO_2 results from only weak physisorption. This feature demonstrates that Cu deposition on ZnO polar surfaces could play an important role in the chemisorption and activation of CO_2.

On the other hand, similar to the case of the clean ZnO (0001) surface, the adsorption of H_2 on the Cu/ZnO(0001) surface was unfeasible (see Table 1), except for the metallic sites. H_2 adsorption on the Cu(111) surface leads to strong chemisorption of H_2 with an adsorption energy of −0.41 eV (see Table 1). Therefore, H_2 adsorption on any of the sites of Cu/ZnO(000$\bar{1}$) could result in the strong chemisorption of H_2. Similar to the cases of H_2 adsorption on the clean ZnO(000$\bar{1}$) surface and Cu/ZnO(000$\bar{1}$), the chemisorption of H_2 on the Cu (111) surface results in the dissociation of H_2. As shown in Fig. 2(l), the two dissociated H atoms are loaded on two neighbouring Cu atoms of the Cu(111) surface (d_{H-Cu} = 1.75 Å). The dissociated H atom might further evolve to the spillover proton among the Cu nano-islands by the photo-generated holes.[41]

Thus, the above results show that Cu deposition on ZnO polar surfaces would promote CO_2 chemisorption on the edge sites of Cu/ZnO(0001) and Cu/ZnO(000$\bar{1}$). These chemisorbed states rarely occur on the clean ZnO polar surfaces. Moreover, Cu deposition on ZnO(0001) could also promote the chemisorption H_2 by inducing the Cu nano-islands on the Cu/ZnO (0001) surface. However, Cu deposition on ZnO(000$\bar{1}$) has a minor effect on the H_2 adsorption, since H_2 adsorption on any of the sites of Cu/ZnO(000$\bar{1}$) could result in the strong chemisorption of H_2. Therefore, when Cu/ZnO(0001) and Cu/ZnO (000$\bar{1}$) are exposed to CO_2 and H_2, the Cu/ZnO(000$\bar{1}$) system could be saturated and poisoned by the strong chemisorption of H_2. In contrast, the adsorption competitors CO_2 and H_2 could be simultaneously chemically adsorbed and activated on Cu/ZnO(0001) (on which the H_2 undergoes chemisorption on metallic sites and CO_2 chemisorption occurs on edge sites). Thus, we propose that Cu/ZnO(0001) is an ideal surface for the hydrogenation of CO_2.

3.2. Electronic structures of the chemisorbed CO_2 states of Cu/ZnO polar surfaces

In this section, detailed electronic structures have been obtained to provide further understanding of the physical and chemical origins of the interaction between CO_2 and the Cu/

ZnO polar surfaces. The ZnO(0001) surface has n-type-like conductivity, as the Fermi level enters into its conduction bands; see the density-of-states (TDOS) (see Fig. S3(a) in ESI†). The ZnO(000$\bar{1}$) surface exhibits p-type conductive characters, as its Fermi level is lower and enters the valence bands (see Fig. S3(c) in ESI†). Similar results were reported in ref. 42 and 43. With Cu deposition on the ZnO(0001) surface, the Cu 3d states contribute to the valence band maxima of the Cu/ZnO (0001) surface, leading the TDOS of the Cu/ZnO(0001) surface to shift to the higher energy level and enlarging its band gap (see Fig. S3(b) in ESI†). In contrast, in the case of Cu/ZnO (000$\bar{1}$), no energy shift of TDOS is found for the Cu/ZnO(000$\bar{1}$) surface. However, the contribution of the Cu 3d orbitals to the valence band maxima is still remarkable in Cu/ZnO(000$\bar{1}$) (see Fig. S3(d) in ESI†). The DOS analysis of the Cu/ZnO polar surface systems reveals that Cu deposition would induce charge redistribution on the interfaces of Cu/ZnO(0001) and Cu/ZnO(000$\bar{1}$).

In the chemisorbed CO_2 states of the Cu/ZnO polar surfaces, the 2p orbitals of the O and C atoms from CO_2 could introduce some states located in the fundamental gaps of these two systems (Fig. 3(a) and (b)). For the chemisorbed CO_2 state of Cu/ZnO(0001), the O(CO_2) 2p orbital hybridizes remarkably with the valence orbitals of Cu in the top of the valence band. The C(CO_2) 2p orbitals contribute to the conduction band, which is mainly dominated by the 4s orbitals of the Zn atoms. In the case of the chemisorbed CO_2 state of the Cu/ZnO(000$\bar{1}$) surface, the O(CO_2) 2p orbital hybridizes with the Cu 3d orbital in the valence band and the surface O 2p in the top of the valence band (ranging from −4.6 to 0.2 eV), while the C(CO_2) 2p contributes to the conduction band in the high-energy-level region (*i.e.*, from 5 to 6 eV). The PDOS results illustrate that there are substantial covalent interactions between CO_2 and the Cu/ZnO polar surface systems, which clearly confirm the formation of chemical bonds between the adsorbed CO_2 and the Cu/ZnO polar surface systems.

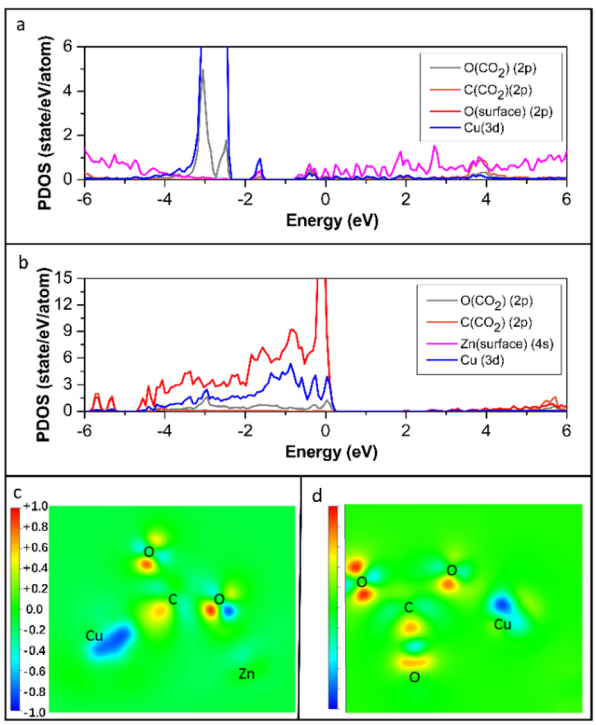

Fig. 3 Partial density of states (PDOS) for (a) CO_2 chemisorption on edge site of Cu/ZnO(0001) and (b) CO_2 chemisorption on edge site of Cu/ZnO(000$\bar{1}$), and contour plots of electronic charge density difference for (c) CO_2 chemisorption on edge site of Cu/ZnO(000$\bar{1}$) and (d) CO_2 chemisorption on edge-site of Cu/ZnO(0001).

Analysis of the electronic density difference (see the contour diagrams in Fig. 3(c) and (d)) again confirms the covalent contribution of the interaction between CO_2 and the Cu/ZnO polar surface system. For the edge sites of Cu/Zn (0001), the charge density changes mainly emerge on the 2p orbitals of the C and O of CO_2, and the Cu atom, as well as the relevant surface Zn atom. Similar charge density changes have been found in the chemisorbed CO_2 states of the Cu/ZnO (000$\bar{1}$) surface, with the charge density changes mainly emerging on the 2p orbitals of C and O of CO_2, the 3d orbitals of the Cu atom, and the 2p orbitals of the linked surface O. The charge density changes of the two Cu/ZnO systems indicate the covalent interaction between CO_2 and the deposited Cu atom. Moreover, the Cu atom donates electrons to CO_2, and the C–O double bonds in CO_2 are greatly weakened and elongated. The depleted charge density of Cu and the accumulated charge density on CO_2 imply that Cu deposition could result in charge redistribution and improve the electron donation ability of ZnO polar surfaces. As a result, the chemisorption of CO_2 is remarkably promoted on the edge-sites of Cu/ZnO polar surfaces.

Bader charge analyses[44,45] were applied to further identify the charge states of CO_2 adsorption on Cu/ZnO polar surfaces (see Table 2). Without CO_2 adsorption, there is significant net negative charge distributed on the Cu atom of Cu/ZnO(0001), indicating that there is electron transfer from ZnO to Cu. This is consistent with our XPS results for Cu/ZnO(0001) (see section 3.4). When CO_2 is adsorbed on the Cu/ZnO(0001), CO_2 gains electrons with a partially negative charge of $-0.9|e|$, which is donated from Cu/ZnO(0001). The Cu atom and the surface Zn atoms of Cu/ZnO(0001) inject electrons to CO_2 with $0.34|e|$ and $0.32|e|$, respectively. In the case of Cu/ZnO(000$\bar{1}$) system, Cu is still the primary electron donor, contributing $0.10|e|$; however, surface O atoms prefer to accept the negative charges of $-0.03|e|$, leading to much less negative partial charges of $-0.04|e|$ in CO_2. This difference in charge transfer in between Cu/ZnO(0001) and Cu/ZnO(000$\bar{1}$) is mainly attributed to their different surface atoms, *i.e.*, the surface Zn atoms of Cu/ZnO(0001) and surface O atoms of Cu/ZnO(000$\bar{1}$), which are characterized by electrophobic and electrophilic properties, respectively, as mentioned in ref. 46.

As a result, Cu deposition on the ZnO polar surface systems would encourage CO_2 activation through its electron donor ability. Moreover, Cu/ZnO(0001) possesses surface Zn atoms with electrophobic properties, which would provide more electron transfer to CO_2 chemisorption than Cu/ZnO(000$\bar{1}$). Thus,

Table 2 Bader charges Q (in $|e|$) of the atoms (or entities) on the clean substrate (*i.e.*, Cu/ZnO) and the adsorbed complex (*i.e.*, CO_2–Cu@ZnO), and their Bader charge differences ΔQ when going from CO_2 in the gas phase plus the clean Cu@ZnO substrate to the adsorbed complex[a]

	CO_2 chemisorbed on Cu/ZnO(0001)				CO_2 chemisorbed on Cu/ZnO(000$\bar{1}$)			
	Cu	Zn[b]	Surface Zn[c]	CO_2	Cu	O[b]	Surface O[c]	CO_2
$Q_{Cu/ZnO}$	−0.31	0.89	6.98	0.00	0.92	−1.07	−7.49	0.00
$Q_{CO_2-Cu/ZnO}$	0.03	1.21	7.08	−0.90	1.02	−1.11	−7.52	−0.04
ΔQ	0.34	0.32	0.10	−0.90	0.10	−0.04	−0.03	−0.04

[a] Negative and positive values of ΔQ indicate electron gain and donation, respectively. [b] For the surface atom involved in the interaction between the adsorbate and substrate. [c] Sum of the charges of all surface atoms in a unit cell except the atom bonding to the CO_2.

Cu/ZnO(0001) could induce more electron transfer to promote the formation of chemisorbed CO_2 species on its edge site than Cu/ZnO(000$\bar{1}$).

3.3. Reaction pathway of CO_2 hydrogenation to formic acid

Based on our previous studies in the above section, Cu/ZnO (0001) is the most feasible candidate for the photocatalytic hydrogenation of CO_2. In this section, the reaction pathway of CO_2 hydrogenation by Cu/ZnO(0001) is investigated. Considering that the H_2 molecule tends to dissociate on Cu nanoislands, we constructed a large-size slab model of Cu_9/ZnO(0001) with a Cu_9 cluster on the ZnO(0001) surface to simulate the CO_2 hydrogenation reaction (see Fig. 1(d) and (c)). The electron location function (ELF) and charge difference distribution calculation of Cu_9/ZnO(0001) reveal that the Cu_9 cluster and ZnO(0001) surface have a strong interaction (Fig. 4(a) and (b)). Much of the electronic charge could be accumulated around the interface of Cu_9 and ZnO(0001), as well as the photogenerated electrons arising from ZnO(0001).

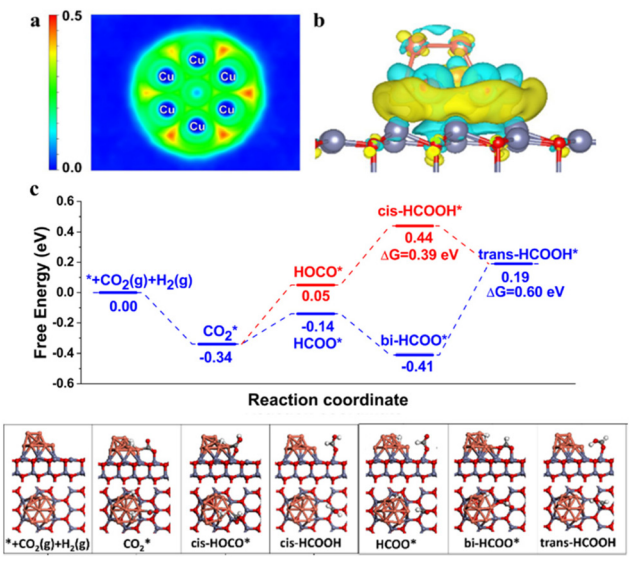

Fig. 4 (a) The electron location function and (b) the differential charge density of the Cu-cluster-loaded ZnO(0001) surface (blue represents positive charge and yellow represents negative charge). (c) The Gibbs free energy diagrams of CO_2 reduction.

This great accumulated charge ability might enhance the reactivity of Cu_9/ZnO(0001) toward the CO_2 reduction.

Fig. 4(c) shows the Gibbs energy profile and intermediate structures of CO_2 hydrogenation by Cu_9/ZnO(0001). The initial step corresponds to the chemisorption of CO_2 on the interface of Cu_9/ZnO(0001). It is energetically favourable to form the exothermic intermediate CO_2* with an energy of −0.3 eV. Here, molecules that have been activated are denoted with a star. Subsequently, the hydrogenation of CO_2* step could generate two different intermediates, HOCO* and HCOO*, due to the fact that the target atom attacked by H can be either the O or C atom of CO_2*. Our calculation results reveal that the formation of both HCOO* and HOCO* are endothermic processes. However, the formation of the intermediate HCOO* requires a smaller activation energy than that of HOCO*. Moreover, since the C atom of CO_2* is combined with the interfacial Cu atom, the C atom could be activated by the greatly accumulated charge around the interface of Cu_9/ZnO(0001). Particularly, in the HCOO* path, the spillover proton on the Cu nano-islands could couple with the photoelectron to attack the C atom of CO_2*, which could greatly promote the formation of the intermediate HCOO*. The intermediate HCOO* is metastable and, subsequently, HCOO* would undergo structural rearrangement to form the bi-HCOO* intermediate with an energetic exothermicity of 0.55 eV. In this structural rearrangement step, the upper O atom of HCOO* would shift to the interface of Cu_9/ZnO(0001) and combine with the interfacial Cu and Zn atoms to form the intermediate bi-HCOO*. In our calculations, bi-HCOO* should overcome a large activation energy to accept another H to form the final product *trans*-HCOOH*. However, the interfacial O atom of bi-HCOO* could be further attacked by the second coupling of a spillover proton and photoelectron, which could promote the process of bi-HCOO* evolving to the final product *trans*-HCOOH*.[29] In view of the HCOO* path, the hydrogenation of CO_2* step and hydrogenation of bi-HCOO* step are both feasible to be assisted by the coupling of a spillover proton and a photoelectron. By contrast, in the hydrogenation of CO_2* step in the HOCO* path, the upper O of CO_2*, as the target of spillover proton attack in the *cis*-HOCO* formation step, is far from the interface of Cu_9/ZnO (0001). Thus, the formation of the intermediate HOCO* is less assisted by the coupling spillover proton and photoelectron near the interface. Therefore, based on our calculations, the

HCOO* path is the optimal reaction pathway for the photocatalytic hydrogenation of CO_2 by Cu/ZnO(0001).

3.4. Experimental study of the direct photocatalytic hydrogenation of CO_2 on the Cu/ZnO(0001) surface

In order to further interpret the above theoretical results and the suggested reaction route of the direct photocatalytic hydrogenation of CO_2 by the Cu/ZnO polar surface, we constructed an illustrative experiment using a custom-built reaction system (see details in the ESI, Fig. S4†). The AFM images of the Cu metal on ZnO substrates are shown in Fig. S5 of the ESI.† Fig. 5(a) and (b) represent the high-resolution Cu $2p_{3/2}$ and O 1s XPS data of the Cu/ZnO(0001), respectively. It can be observed that when Cu was deposited on the ZnO(0001), the binding energy of Cu $2p_{3/2}$ shifted to a lower value, indicating an electron transfer process from ZnO(0001) to Cu, which agrees with the above theoretical Bader charge analysis. Correspondingly, the O 1s binding energy of the Cu-loaded ZnO(0001) surface shows an upward shift compared to that of the clean ZnO(0001) surface. The fed H_2 and CO_2 gases reacted on the clean ZnO or Cu/ZnO polar surface under the radiation of a 300 W xenon lamp. After 4 hours of reaction, the irradiated surfaces of the photocatalysts were dried in a vacuum oven at 60 °C and then scraped with a razor blade to obtain the residual reaction products. The powders scraped from the reacted catalyst surface were then analysed using infrared (IR) transmission spectroscopy. Fig. 5(c) presents the FT-IR spectrum of the surface product on Cu/ZnO(0001) after reaction. The characteristic peaks located at 2970, 2880, 2740, 1668, 1580, 1397, 1378, and 1353 cm^{-1} are in good agreement with those of zinc formate,[47] while the characteristic peaks of copper formate (at 2930, 2850, 1620, and 1350 cm^{-1}) are absent.[48] Thus, it can be

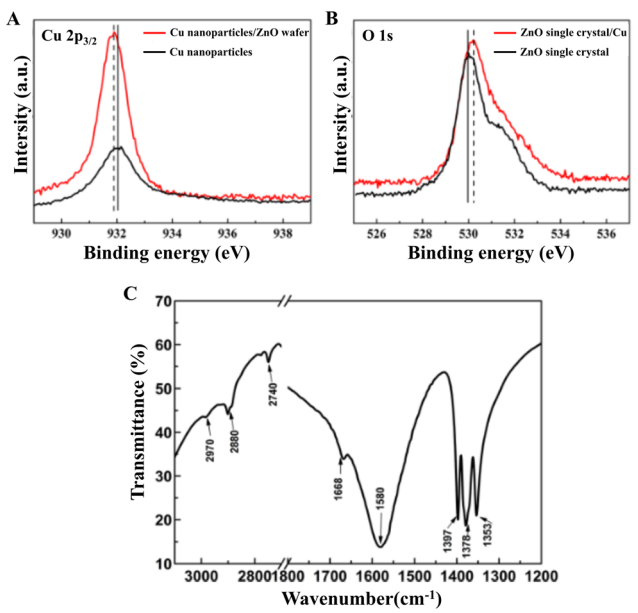

Fig. 5 (a) XPS Cu $2p_{3/2}$ and (b) O 1s core level spectra; (c) IR spectrum data of the Cu/ZnO(0001) catalyst after the photocatalytic reaction.

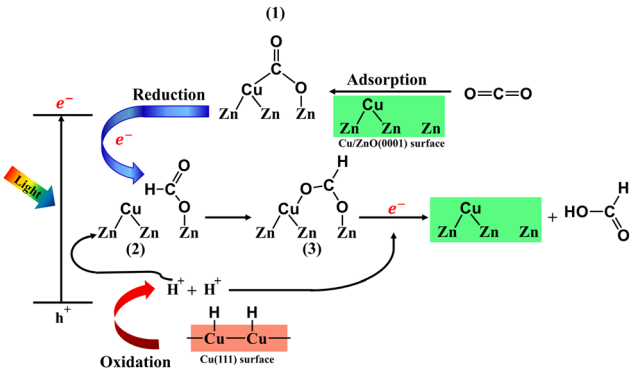

Fig. 6 The proposed schematic illustration of the reaction route of the direct photocatalytic hydrogenation of CO_2 on the Cu/ZnO(0001) surface.

speculated that formic acid is a possible reduction product of the photocatalytic hydrogenation of CO_2 on the Cu/ZnO polar surface. However, for the clean ZnO and Cu/ZnO(000$\bar{1}$) photocatalysts, no obvious products related to the reduction of CO_2 can be identified in the scraped powders from the FTIR spectrum. Therefore, the Cu/ZnO(0001) surface is an efficient photocatalyst for the direct hydrogenation of CO_2, which is consistent with the above theoretical discussions.

Combining the theoretical and experimental works, we propose the optimal reaction route of the direct photocatalytic hydrogenation of CO_2 by Cu/ZnO(0001) as illustrated in Fig. 6. In the oxidation half-reaction, an H_2 molecule is adsorbed by Cu nanoislands and then is bound to a Cu atom after disassociation. These two disassociated H atoms are further oxidized to two H^+ by the photo-generated holes. In the reduction half-reaction, CO_2 is absorbed at the edge site of Cu/ZnO(0001) and becomes a bidentate carbonate structure (intermediate CO_2*, structure (1) in Fig. 6). The intermediate CO_2* is then attacked by H^+ coupling with a photoelectron on the interface, *via* simultaneous C–Cu bond cleavage and C–H bond formation steps, resulting in the HCOO* intermediate (structure (2) in Fig. 6). The intermediate HCOO* is metastable, and it is energetic favourable for it to undergo structural rearrangement to form the intermediate bi-HCOO* (structure (3) in Fig. 6). Finally, the secondly spillover proton coupled with the photoelectron would attack the interfacial O of the bi-HCOO* intermediate, leading to the final *trans*-HCOOH* product (formic acid).

4. Conclusions

In this paper, the adsorption of CO_2 and H_2 on the polar surfaces of ZnO(0001), ZnO(000$\bar{1}$), Cu/ZnO(0001), and Cu/ZnO (000$\bar{1}$) have been systematically investigated using DFT simulations. Our calculations showed that CO_2 can only be weakly physisorbed on clean ZnO(0001) and ZnO(000$\bar{1}$) polar surfaces. In contrast, the Cu deposited on the ZnO polar surfaces Cu/ZnO(0001) and Cu/ZnO(000$\bar{1}$) could greatly promote the chemical adsorption of CO_2 on the surfaces. The electronic

structure studies clearly show that Cu deposition induces charge redistribution on the Cu/ZnO polar surfaces and improves the charge donor ability of the ZnO substrate near Cu atoms, and thereby the chemical adsorption of CO_2 on Cu/ZnO(0001) is enhanced. H_2 prefers to chemisorb on the deposited Cu nanoislands, ZnO(000$\bar{1}$) surface and Cu/ZnO(000$\bar{1}$). Therefore, when Cu/ZnO(0001) and Cu/ZnO(000$\bar{1}$) are exposed to CO_2 and H_2, Cu/ZnO(000$\bar{1}$) could be saturated and poisoned by the strong chemisorption of H_2, while, in contrast, Cu/ZnO(0001) has more opportunity to adsorb H_2 and CO_2 simultaneously near the edge site to promote the hydrogenation of CO_2. Thus, it can be deduced that Cu/ZnO(0001) should be a favourable surface for the photocatalytic hydrogenation of CO_2. This deduction is then confirmed by the photocatalytic hydrogenation experiment. The optimal HCOO* reaction pathway for the photocatalytic hydrogenation of CO_2 by Cu/ZnO(0001) is proposed based on the theoretical and experimental results. In this optimal HCOO* path, the hydrogenation of CO_2* step and hydrogenation of HCOO* step could be promoted by the coupling of a photo-generated spillover proton and a photoelectron on the interface of Cu/ZnO(0001). This research demonstrated the feasibility of the photocatalytic reduction of CO_2 on Cu/ZnO(0001), and will be helpful for the reasonable design of high-efficiency catalysts.

Author contributions

Han Xiao carried out the DFT calculations and analysed the data. Yihong Lian and Shiduo Zhang performed Bader charge analyses and calculated the electronic location function. Jiye Zhang conducted the experiments. Minyi Zhang and Chunsen Li designed the project, analysed the data, and wrote the manuscript.

Conflicts of interest

There are no conflicts to declare.

Acknowledgements

This investigation was based on work supported by the National Natural Science Foundation of China (Grant No. 21933009 and 51472241) and the Natural Science Foundation of Fujian Province (Grant No. 2021J01525).

References

1 E. J. Carrington, C. A. McAnally, A. J. Fletcher, S. P. Thompson, M. Warren and L. Brammer, *Nat. Chem.*, 2017, **9**, 882–889.
2 F. Zha, J. Ding, Y. Chang, J. F. Ding, J. Y. Wang and J. Ma, *Ind. Eng. Chem. Res.*, 2012, **51**, 345.
3 F. C. Meunier, *Angew. Chem., Int. Ed.*, 2011, **50**, 4053.
4 P. Gao, S. G. Li, X. A. Bu, S. S. Dang, Z. Y. Liu, H. Wang, L. S. Zhong, M. H. Qiu, C. G. Yang, J. Cai, W. Wei and Y. H. Sun, *Nat. Chem.*, 2017, **9**, 1019–1024.
5 S. Patial, R. Kumar, P. Raizada, P. Singh, Q. V. Le, E. Lichtfouse, D. L. T. Nguyen and V. H. Nguyen, *Environ. Res.*, 2021, **197**, 111134.
6 R. G. Zhang, H. Y. Liu, B. J. Wang and L. X. Ling, *Appl. Catal., B*, 2012, **126**, 108.
7 S. A. Kondrat, P. J. Smith, J. H. Carter, J. S. Hayward, G. J. Pudge, G. Shaw, M. S. Spencer, J. K. Bartley, S. H. Taylora and G. J. Hutchings, *Faraday Discuss.*, 2017, **197**, 287–307.
8 X. Li, J. Q. Wen, J. X. Low, Y. P. Fang and J. G. Yu, *Sci. China Mater.*, 2014, **57**, 70–100.
9 M. Marszewski, S. W. Cao, J. G. Yu and M. Jaroniec, *Mater. Horiz.*, 2015, **2**, 261–278.
10 Q. J. Xiang, B. Cheng and J. G. Yu, *Angew. Chem., Int. Ed.*, 2015, **54**, 11350–11366.
11 E. S. Jang, J. H. Won, S. J. Hwang and J. H. Choy, *Adv. Mater.*, 2006, **18**, 3309.
12 N. Kislov, J. Lahiri, H. Verma, D. Y. Goswami, E. Stefanakos and M. Batzill, *Langmuir*, 2009, **25**, 3310.
13 H. Fatima, M. R. Azhar, Y. J. Zhong, Y. Arafat, M. Khiadani and Z. P. Shao, *J. Colloid Interface Sci.*, 2022, **614**, 538–546.
14 A. X. Wang, W. J. Wang, J. Y. Chen, R. D. Mao, Y. P. Pang, Y. G. Li, W. Chen, D. C. Chen, D. Hao, B. J. Ni, M. Saunders and G. H. Jia, *J. Phys. Chem. Lett.*, 2020, **11**, 4990–4997.
15 L. Y. Yang, S. Y. Dong, J. H. Sun, J. L. Feng, Q. H. Wu and S. P. Sun, *J. Hazard. Mater.*, 2010, **179**, 438.
16 S. He, S. T. Zhang, J. Lu, Y. F. Zhao, J. Ma, M. Wei, D. G. Evans and X. Duan, *Chem. Commun.*, 2011, **47**, 10797.
17 A. Mclaren, T. Valdes-Solis, G. Q. Li and S. C. Tsang, *J. Am. Chem. Soc.*, 2009, **131**, 12540.
18 Q. S. Guo, Q. H. Zhang, H. Z. Wang, Z. F. Liu and Z. Zhao, *Catal. Commun.*, 2016, **77**, 118–122.
19 X. Y. He, M. Liu, Z. Liang, Z. Y. Wang, P. Wang, Y. Y. Liu, H. F. Cheng, Y. Dai, Z. K. Zheng and B. B. Huang, *J. Solid State Chem.*, 2021, **298**, 122113.
20 D. Weibel, Z. R. Jovanovic and A. Steinfeld, *Chem. Eng. Sci.*, 2017, **165**, 96–107.
21 M. Dorraja, M. Alizadehb, N. A. Sairia, W. J. Basiruna, B. T. Gohd, P. M. Woia and Y. Aliasa, *Appl. Surf. Sci.*, 2017, **414**, 251–261.
22 Y. Zhang, Y. J. Ji, J. Li, H. Z. Liu, Z. Y. Zhong and F. B. Su, *J. Catal.*, 2017, **348**, 233–245.
23 S. Singh, R. Pendurthi, M. Khanuja, S. S. Islam, S. Rajput and S. M. Shivaprasad, *Appl. Phys. A*, 2017, **123**, 184.
24 R. Gleißner, H. Noei, S. M. Chung, G. D. L. Semione, E. E. Beck, A. C. Dippel, O. Gutowski, G. Gizer, V. Vonk and A. Stierle, *J. Phys. Chem. C*, 2021, **125**, 23561–23569.
25 F. Jiang, Y. Yang, L. Wang, Y. F. Li, Z. H. Fang, Y. B. Xu, B. Liu and X. H. Liu, *Catal. Sci. Technol.*, 2022, **12**, 551–564.
26 R. C. Pawar, D. H. Choi, J. S. Lee and C. S. Lee, *Mater. Chem. Phys.*, 2015, **151**, 167–180.

27 F. L. Liao, Y. Q. Huang, J. W. Ge, W. R. Zheng, K. Tedsree, P. Collier, X. L. Hong and S. C. Tsang, *Angew. Chem., Int. Ed.*, 2011, **50**, 2162–2165.
28 R. Narayanan and M. A. El-Sayed, *J. Phys. Chem. B*, 2005, **109**, 12663–12676.
29 Q. L. Tang, W. T. Zou, R. K. Huang, Q. Wang and X. X. Duan, *Phys. Chem. Chem. Phys.*, 2015, **17**, 7317–7333.
30 M. D. Higham, D. Mora-Fonz, A. A. Sokol, S. M. Woodley and C. R. A. Catlow, *J. Mater. Chem. A*, 2020, **8**, 22840–22857.
31 G. Kresse and J. Furthmüller, *Phys. Rev. B: Condens. Matter Mater. Phys.*, 1996, **54**, 11169.
32 G. Kresse and J. Furthmüller, *Comput. Mater. Sci.*, 1996, **6**, 15.
33 P. E. Blöchl, *Phys. Rev. B: Condens. Matter Mater. Phys.*, 1994, **50**, 17953–17979.
34 J. P. Perdew, K. Burke and M. Ernzerhof, *Phys. Rev. Lett.*, 1996, **77**, 3865.
35 H. Li, L. K. Schirra, J. Shim, H. Cheun, B. Kippelen, O. L. A. Monti and J. L. Bredas, *Chem. Mater.*, 2012, **12**, 3044.
36 Q. L. Tang, W. T. Zou, R. K. Huang, Q. Wang and X. X. Duan, *Phys. Chem. Chem. Phys.*, 2015, **17**, 7317.
37 W. W. Lin, D. G. Chen, J. Y. Zhang, Z. Lin, J. K. Huang, W. Li, Y. H. Wang and F. Huang, *Cryst. Growth Des.*, 2009, **9**, 4378.
38 A. N. Mariano and R. E. Hanneman, *J. Appl. Phys.*, 1963, **34**, 384.
39 E. H. Kisi and M. M. Elcombe, *Acta Crystallogr., Sect. C: Cryst. Struct. Commun.*, 1989, **45**, 1867.
40 Q. L. Tang and Q. H. Luo, *J. Phys. Chem. C*, 2013, **117**, 22954.
41 F. Jiang, Y. Yang, L. Wang, Y. F. Li, Z. H. Fang, Y. B. Xu, B. Liu and X. H. Liu, *Catal. Sci. Technol.*, 2022, **12**, 551–564.
42 L. Qiao, Y. Zeng, C. Q. Qu, H. Z. Zhang, X. Y. Hu, L. J. Song, D. M. Bi and S. J. Liu, *Phys. E*, 2013, **48**, 7.
43 L. Qiao, Y. Zeng, C. Q. Qu, X. Y. Hu, L. J. Song, S. J. Liu and Y. M. Sui, *Nano*, 2014, **9**, 1450006.
44 R. F. W. Bader, *Acc. Chem. Res.*, 1985, **18**, 9.
45 G. Henkelman, A. Arnaldsson and H. Jónsson, *Comput. Mater. Sci.*, 2006, **36**, 354.
46 C. T. Au, W. Hirsch and W. Hirschwald, *Surf. Sci.*, 1988, **197**, 391.
47 S. Fujita, M. Usui, H. Ito and N. Takezawa, *J. Catal.*, 1995, **157**, 403–413.
48 W. R. A. M. Robinson and J. C. Mol, *Appl. Catal., A*, 1993, **98**, 81–97.